I&EC research
Industrial & Engineering Chemistry Research

pubs.acs.org/IECR

Article

Sodium Hydroxide-Based CO_2 Direct Air Capture for Soda Ash Production—Fundamentals for Process Engineering

Somayyeh Ghaffari,* Maria F. Gutierrez, Andreas Seidel-Morgenstern, Heike Lorenz, and Peter Schulze

Cite This: *Ind. Eng. Chem. Res.* 2023, 62, 7566−7579

Read Online

ACCESS | Metrics & More | Article Recommendations | Supporting Information

ABSTRACT: This work introduces the principles and supplies the first key parameters for replacing the conventional ammonia-soda (Solvay) process with a new environmentally friendly and sustainable process. For this, the absorption of diluted CO_2 (0.0153−1.2 vol %) in carbonated NaOH solutions was experimentally studied in a temperature range relevant for direct air capture (DAC) in the middle Europe (5−20 °C). A dynamic process model was formulated and solved based on the literature parameters. It was found that by refitting the parameters, the average error was reduced from 9.49 to 7.8%. The absorption performance was evaluated using the mass transfer coefficient (K_{G,CO_2}), which is considered as a useful parameter for the future process design. The mass transfer coefficient reaches a maximum amount of about 3 mm/s at around 6 wt % NaOH, 0 wt % Na_2CO_3, 20 °C, and 500 ppm CO_2. The effects of NaOH and Na_2CO_3 concentrations and temperature on the mass transfer coefficient were experimentally and theoretically studied. Considering all effects simultaneously, the design aspects for an efficient NaOH-based CO_2 DAC process for Na_2CO_3 production are concluded, in which K_{G,CO_2} decreases with rising temperature while operating at saturated ion concentrations of Na_2CO_3.

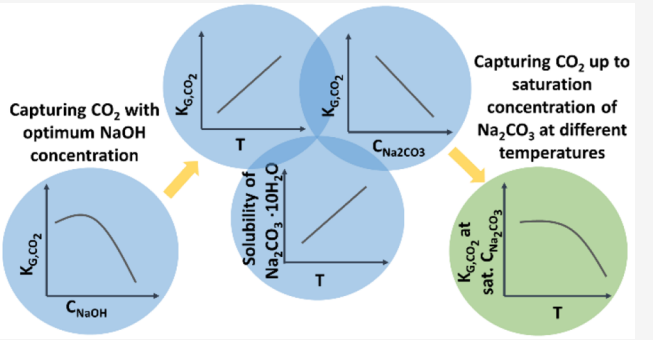

1. INTRODUCTION

Global warming is the long-term heating of earth's climate system observed since the pre-industrial period due to the human activities.[1] According to the Intergovernmental Panel on Climate Change (IPCC), to stabilize the atmospheric CO_2 level between 300 and 450 part per million by volume (ppmv) by 2050, CO_2 emissions must be reduced by about 30−80%.[2] However, capturing 80% of CO_2 emissions cannot be achieved even if all point source emissions are captured.[3] Therefore, capturing nonpoint source emissions of CO_2 using direct air capture (DAC) systems is necessary in both carbon capture and storage (CCS) and carbon capture and utilization (CCU). Although, the physical utilization of CO_2 is well-established in the beverage industry, for fire extinguishers, in the textile sector, in the food industry, and in enhanced oil/gas recovery, there are a lot of uncovered sectors and additional opportunities in its chemical utilization including producing inorganic carbonates like soda ash (sodium carbonate anhydrate).

Nearly half of the worldwide annual production of 56 million metric tons of soda ash, used in glass, chemicals, soaps, detergents, metallurgy, water treatment, pulp, and paper is produced by the classical ammonia-soda (Solvay) process.[4] This process, which has been applied for more than 150 years, can be considered as a fully optimized process. However, it emits significant amounts of fossil CO_2 and generates waste streams containing potentially hazardous substances.[5] The Carbon-negative sODA ash (CODA) project is intended to establish the foundation for replacing the conventional Solvay process with a new environmentally friendly process that produces soda ash in a more sustainable and climate-positive manner. The CODA process is an integration of three subprocesses: first, sodium hydroxide generation by electrolysis of rock salt brine using renewable energy; second, CO_2 absorption directly from air; and third, anhydrous soda ash crystallization with the corresponding downstream processes. Figure 1 illustrates the overall concept of the CODA process.

In comparison to the ammonia-soda process, emissions totaling around 900 kg of CO_2 per ton of produced soda ash can be theoretically avoided (around 500 kg by carbon direct avoidance (CDA)) and absorbed (around 400 kg by CCU) by the CODA process. Besides, it produces hydrogen and chlorine as valuable byproducts of the electrolysis or hydrogen chloride via bipolar electrodialysis.

Received: February 5, 2023
Revised: April 24, 2023
Accepted: April 25, 2023
Published: May 7, 2023

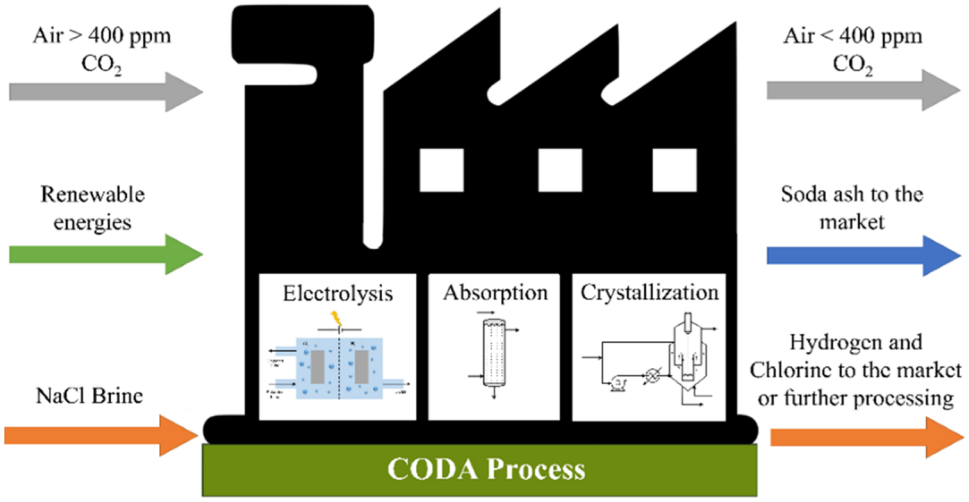

Figure 1. Concept of the envisaged CODA process. Air, NaCl brine, and renewable electricity are used to produce CO_2-depleted air, soda ash, and chlorine and hydrogen that may be marketed or further processed.

A particular challenge in the development of the CODA process is its strong dependence on weather conditions. The generation of renewable electricity from the sun and the wind is just as dependent on the weather as the CO_2 direct air capture on the air humidity and temperature, which subsequently has an impact on the soda ash crystallization. Therefore, the whole process must be adaptable to the weather conditions through a large operation window. At the earliest stage of the CODA project, the absorption of CO_2 in a sodium hydroxide solution has been fundamentally studied both theoretically and experimentally and will be the subject of this paper.

The mechanism of CO_2 absorption in the aqueous NaOH solution can be explained with the following reactions. First, gaseous CO_2 is physically absorbed (eq 1), which instantly reacts with a sodium hydroxide ion (OH^-) to generate a bicarbonate ion (HCO_3^-) (eq 2), that is further converted with another OH^- to a carbonate ion CO_3^{2-} (eq 3). The overall reaction taking place in the liquid phase is given in eq 4. 4eeeeq 4.

$$CO_{2(g)} \rightarrow CO_{2(aq)} \quad (1)$$

$$CO_{2(aq)} + OH^-_{(aq)} \leftrightarrow HCO_3^-{}_{(aq)} \quad (2)$$

$$HCO_3^-{}_{(aq)} + OH^-_{(aq)} \leftrightarrow CO_3^{2-}{}_{(aq)} + H_2O \quad (3)$$

$$CO_{2(aq)} + 2NaOH_{(aq)} \leftrightarrow Na_2CO_{3(aq)} + H_2O \quad (4)$$

In the literature, studies on the absorption of carbon dioxide by sodium hydroxide solution with different absorption contactors, like spray-based contactor,[6] batch reactor with sparger,[7,8] packed tower,[9−11] spray dryer,[12] membrane contactor,[10] and airlift reactor[13] are reported. Although most of these works have used a much higher range of CO_2 concentration (10−100 vol %), few have studied the absorption of CO_2 directly from air.[6,9] Table 1 gives an overview of these works with more details. The published works focus on the description of industrial-scale equipment and its evaluation in technical and energetic terms. Most of the process feasibility indicators have been obtained from experiments and simplified modeling or simulations performed with commercial software (no detailed models have been provided). In most of the mentioned works, the formed sodium carbonate is processed in a regeneration stage to obtain pure CO_2 as the target product. However, the goal of the CODA project is to crystallize sodium carbonate as the target product from the stream obtained by absorption, which leads to specific "CODA conditions" for the absorption process, namely, up to saturated carbonate concentrations, mean temperature of 10 °C (for the middle Europe), and 400 ppm of CO_2 concentration.

From the chemical engineering literature, the size of an absorber is related to the height of a transfer unit (H_{OG}), which depends on the overall mass transfer coefficient (K_G) and the specific surface area for mass transfer (a_e). Both parameters depend on the operational conditions, physical properties, and geometry of the used equipment. The process design and the used equipment relies on the determination of the aforementioned parameters, which is commonly done by experimentation. If the absorber is designed based on a commercially available technology, empirical correlations for the calculation of K_G and a_e are given by the vendors. In CO_2 absorption, the determination of K_G is particularly challenging, given the reactive nature of the absorption.

Few studies about CO_2 DAC using sodium hydroxide have been published,[14,15] in which the main decisions on the operational conditions (e.g., NaOH concentration, temperature) have not been discussed in details. For example, the detailed design of an air−liquid contactor for large-scale capture of CO_2 from air was done using a nonpublished empirical function for predicting the overall mass transfer coefficient.[16] Although the effect of NaOH on K_G for CO_2 DAC has been briefly considered,[6,17] the effect of temperature and the concentration of Na_2CO_3 on K_G has not been analyzed in the open literature to the best of the authors' knowledge.

To obtain the foundations of the absorption of airborne CO_2 by carbonated NaOH solutions, a semi-batch stirred tank reactor was used to study the process at near-atmospheric CO_2 concentrations, different NaOH and Na_2CO_3 concentrations, temperatures, and well-defined mass transfer areas. In contrast to previous studies, in this simple-designed setup, the mass transfer area was changed with a higher certainty. Typical experimental absorption studies determine either K_Ga_e for a specific equipment,[13] K_G based on a previously determined

https://doi.org/10.1021/acs.iecr.3c00357
Ind. Eng. Chem. Res. 2023, 62, 7566−7579

Table 1. Overview of CO_2 Capture in Aqueous NaOH Solution from Ambient and Higher Concentrated CO_2[a]

contactor and capturing mode	CO_2 conc. (vol %)	NaOH conc. (wt %)	Na_2CO_3 (wt %)	temperature (°C)	products	main experimental results	main modeling results	year and reference
spray-based contactor co-current	0.04 directly from air	1.4, 5.32, and 20	0	15 (65% RH) and 19 (50% RH)	not analyzed	3.7 mmol CO_2/L of solution per pass (0.4 ton-CO_2/year per m^2 of the contactor cross-section)	gas-side mass transfer resistance was neglected; reaction rate and Henry's constant were calculated using the activity coefficient	2008[6]
packed column counter-current	0.04 directly from air	1.2	0	NA	sodium carbonate (decahydrate and anhydrous)	removal efficiency: 68%	process simulation with VMGSim, Visio, and Excel; no details given	2009[9]
disks contactor (SDC)	0.18−0.30	0.05−7.5	5−10	25−50	not analyzed	removal efficiency was not discussed	reaction rate parameters obtained for a first-order expression with respect to NaOH; Henry's constant obtained from the literature	2015[18]
spray dryer	0−100	1−3	0	50, 75, and 100	not analyzed	maximum removal efficiency: 63%	reaction rate parameters obtained for a first-order expression with respect to NaOH	2016[12]
packed column counter-current	10−15	0.8−4	0−5*	NA	carbonate and bicarbonate	maximum removal efficiency: 90−100%	NA	2018[10]
membrane contactor counter-current	10−15	0.8−4	0−5*	NA	carbonate and bicarbonate	maximum removal efficiency: 70−80%	NA	2018[10]
three packed column reactors connected in a series	14	15	NA	NA	carbonate and bicarbonate	maximum total absorption rate: above 95%	NA	2016[11]
airlift reactor								
counter-current	20	0.4	0.4*	25	carbonate and bicarbonate	maximum volumetric mass transfer: 0.016 s^{-1}	gas-side mass transfer resistance was neglected; reaction rate was calculated using the activity coefficient; parameters from the literature were used	2020[13]
tubular reactor with woven meshed mixer Cu-current	30	up to 0.28 wt %	0.03*	NA	carbonate	removal efficiency of 95%	NA	2022[19]
batch-typed pyrex reactor with a sparger	31.5	1−5	0−6.5*	25	carbonates, bicarbonate, and trona	capture efficiency: about 59%	NA	2012[8]
batch reactor with a porous ceramic bubble sparger	45 from a landfill gas	0.4 and 0.8 plus wastewater	0.4−0.8*	constant room temperature	powder of ammonia bicarbonate, carbonic acid, carbonate, and bicarbonate anions	maximum CO_2 loading: 1.7 mol CO_2/L	NA	2009[7]
absorption tube provided with a stirrer	100	up to 26	0	30	carbonate	maximum absorption rate: 3 mL CO_2/min/cm^2	parameters obtained to describe the initial absorption rate as a function of the NaOH concentration and liquid viscosity	1934[20]

[a]RH: Relative humidity. *Produced carbonate (not added). NA: Not available.

https://doi.org/10.1021/acs.iecr.3c00357
Ind. Eng. Chem. Res. 2023, 62, 7566−7579

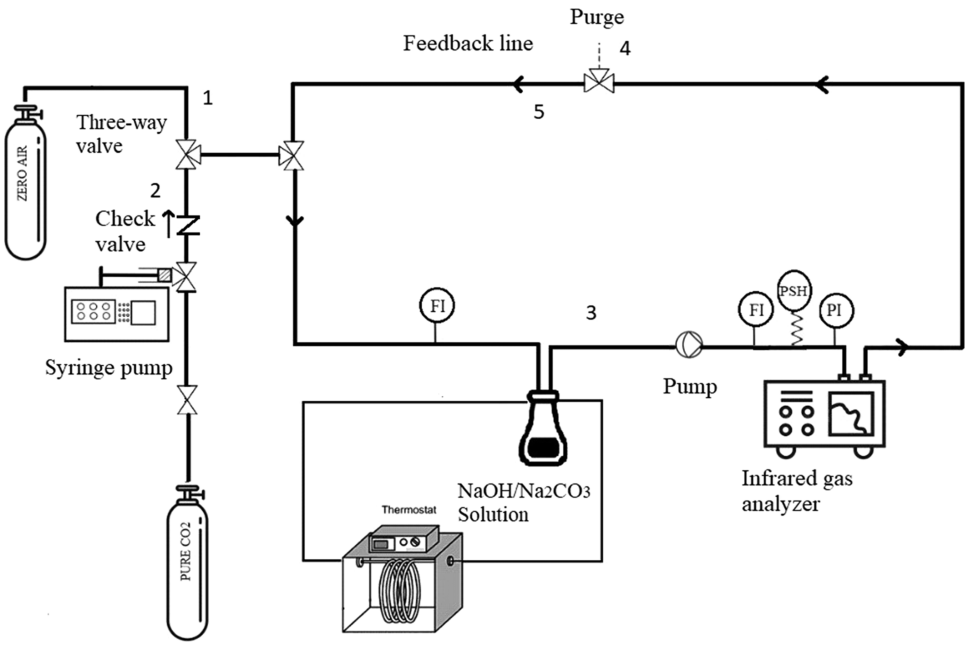

Figure 2. Schematic diagram of the setup used to absorb CO_2 in a fed-batch closed-loop system.

correlation or modeled a_e,[6] or a_e based on a theoretical correlation of K_G.[21] The setup used in this study allows analyzing the effect of different operational variables on K_G without the need for complex empirical correlations or models to determine the mass transfer area. The absorption is evaluated by means of the steady-state concentration of CO_2 in the gas phase and the derived mass transfer coefficient. The experimental values are compared to results obtained with a model built using the kinetic and the phase equilibrium parameters of the literature that were derived from "non-CODA" conditions in terms of CO_2 and carbonate concentrations and temperature. The influence of NaOH and Na_2CO_3 concentrations and temperature on the mass transfer coefficient are discussed, as well as its implications on the process design. Additionally, the model parameters are refitted for "CODA conditions". The model can be used to calculate K_G in more complex equipment, where effort is needed for the determination of a_e. Moreover, the results of this study allow us to identify an optimal NaOH concentration and quantify the influence of Na_2CO_3 and temperature on the absorption.

2. MATERIALS AND METHODS

2.1. Materials. NaOH (pellets) with 99.0% purity was purchased from Merck company, Germany, and the zero air (20.5 vol % O_2, rest N_2, zero CO_2) and CO_2 with a purity of 99.9% from Westfalen company. Deionized water from a Milli-Q system (Merck) was used in all of the experiments.

2.2. Experimental Methods. A fed-batch system was designed to absorb CO_2 in a reactor partly filled with a NaOH/Na_2CO_3 solution, in which CO_2 was continuously fed to the closed-loop system. This setup mainly consisted of two sources of gases (zero air (synthetic air without CO_2) and pure CO_2), a CO_2/H_2O gas analyzer (LI-850 from LiCor, Cambridge, U.K.), which also measures gas temperature and pressure, two gas flow meters, a syringe pump for feeding CO_2, a thermostat for temperature control of the solution, valves for flow control, and reactors. The latter were laboratory bottles made from borosilicate 3.3 glass with a GL45 screw cap and different volumes between 100 and 1000 mL as well as different liquid surface areas (inner bottle diameters) (see Figure 2 and Section S.8).

In each experiment, (a) initially zero air was used through line 1 to purge the system to remove CO_2 and water from the system. After reaching dry and CO_2-free conditions, the zero air line 1 and the purging line 4 were closed, and the feedback line 5 was opened while the elevated pressure was recorded by the gas analyzer to check the system for leakage. After some time, the initial pressure of the system was set close to 100 kPa (atmospheric pressure) by shortly venting the purge valve and kept constant for the all experiments. The gas in the closed loop (lines 3−5) was circulated through the absorption bottle and the gas analyzer by the membrane pump within the gas analyzer at a defined flow rate of about 700 mL/min, except in some experiments where it is stated differently.

Next, (b) a flow of pure CO_2 was fed by a syringe pump with a defined flow rate (e.g., 1, 0.7, 0.5, 0.3, or 0.15 mL/min) through line 2 into the circulating flow of the closed loop and is diluted to the desired concentration before reaching the reactor containing a known mass and composition of the NaOH/Na_2CO_3 solution. The difference between the measured CO_2 concentration at the absorber outlet and the CO_2-enriched inlet can be estimated to be between 219 and 1428 ppm (=0.15 and 1 mL of CO_2/min/700 mL of gas/min), depending on the actual CO_2 feed rate. The experimental error can be estimated to be the average between the inlet and outlet concentration difference, namely, about +100 and +700 ppm, at 0.15 and a 1 mL/min of CO_2 feed rate, respectively (assuming perfect mixing of the gas phase in the reactor overhead). A check-valve was applied in line 2 to prevent the premixing of gases inside the loop with CO_2 inside the syringe pump. The stirring speed of the NaOH/Na_2CO_3 solution was limited to 300 rpm to have a plane and defined liquid surface as a mass transfer area.

Finally, (c) after some minutes, a steady-state concentration of CO_2 in the circulation loop was reached, meaning that the CO_2 feed and CO_2 absorption reached the same rate. Due to

https://doi.org/10.1021/acs.iecr.3c00357
Ind. Eng. Chem. Res. 2023, 62, 7566−7579

the low CO_2 feed rates and relatively large solution volume and concentration, the change in OH^- and CO_3^{2-} concentrations due to the reaction of OH^- with CO_2 to CO_3^{2-} was neglectable (less than 0.1 wt %) within the time of the experiment. The flow rate of pure CO_2 was changed in a step-like way to obtain the corresponding steady-state CO_2 concentration. This procedure was repeated for the different $NaOH/Na_2CO_3$ solutions and sizes of reactors with different mass transfer areas. A thermostat was used for temperature control of the reactor and to prevent condensation of water droplets inside the tubes (reactor limited to room temperature ~23 °C). A pressure meter and PSH (safety pressure release valve) were installed to protect the analyzer's gas cell against high pressures. A photograph of the setup is presented in Section S.8. The experimental mass transfer coefficient (given in units of mm/s) was calculated as the quotient of molar CO_2 feed rate (mol/s), the product of mass transfer area (m^2), and steady-state CO_2 concentration (mol/m^3) (see eq 28).

Since the maximum allowed flow rate for the used gas analyzer is 1 L/min, another version of the experimental setup was used to investigate the effect of the circulating flow rate on absorption. Therefore, in this version of the setup, two loops were designed; one was an absorption loop, in which flow rates (between 0.4 and 1.6 L/min) were maintained using a second membrane pump. The other loop connected the gas analyzer, in which the pump inside the analyzer circulated the gas. The same procedure as described above was used for absorption experiments in this setup. A schematic of this setup can be found in Section S.1, Supporting Information (SI).

Experimental and analysis errors were minimized by the following measures. The used syringe pump was calibrated with a bubble flow meter (HORIBASTEC VP-2), and the CO_2 analyzer (LI-COR 850) was calibrated and has an error of about ± 1%. It should be noted that the hygroscopic behavior of NaOH can decrease its purity while handling, and therefore, there is a small uncertainty on its concentration.

2.3. Theoretical Methods. A dynamic model based on the material balances of the gas and liquid phases can describe the absorption of CO_2 in the experimental system. Two control volumes were analyzed, one for each phase present in the system. These control volumes, as well as the material streams entering each volume, are shown in Figure 3. It is worth noting that the gas phase control volume depicted in Figure 3 includes not only the gas space above the solution inside the reactor but also the tubings and gas analyzer (optical cell inside gas analyzer) volumes shown in Figure 2.

The overall CO_2 and H_2O mass balances in the gas phase are presented in eqs 5−7, where S is the mass transfer area (cross-sectional area of each size of bottle obtained by measuring its inner diameter), $\dot{F}_{in}$ is the inlet molar flow rate, and $\dot{N}$ is the molar flux. The total number of moles in the gas phase (n_G) was calculated as a function of pressure (P), temperature (T), and volume of the gas phase (V_G) in the system using the ideal gas assumption eq 8. The volume of the gas phase was determined by a simple experiment shown in Section S.4, Supporting Information. The CO_2 concentration of the feed gas ($y^{in}_{CO_2}$) was always 1 because the feed gas was pure CO_2.

$$\frac{dn_G}{dt} = \dot{F}_{in} - \dot{N}_{CO_2}S + \dot{N}_wS \tag{5}$$

$$n_G\frac{dy_{CO_2}}{dt} = y^{in}_{CO_2}\dot{F}_{in} - \dot{N}_{CO_2}S - y_{CO_2}\frac{dn_G}{dt} \tag{6}$$

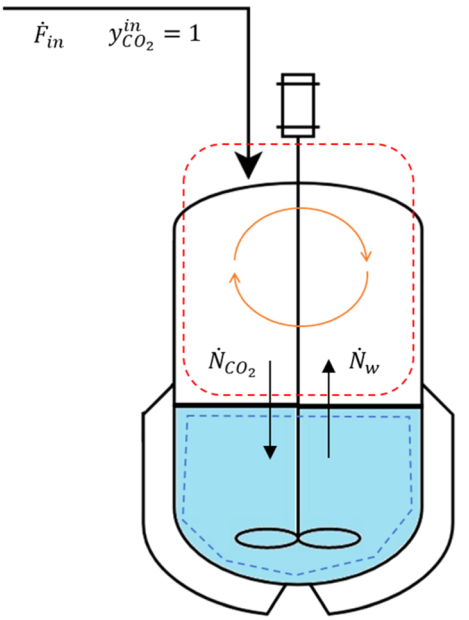

Figure 3. Illustration of the experimental setup used for modeling the absorption of CO_2 using $NaOH/Na_2CO_3$ solutions (gas control volume: red; liquid control volume; blue).

$$n_G\frac{dy_w}{dt} = y^{in}_w\dot{F}_{in} + \dot{N}_wS - y_w\frac{dn_G}{dt} \tag{7}$$

$$n_G = \frac{PV_G}{RT} \tag{8}$$

The CO_2 flux from the gas into the liquid phase ($\dot{N}_{CO_2}$) is calculated from the overall gas mass transfer coefficient (K_{G,CO_2}) and the gas concentration gradient (assuming that the interphase is in equilibrium with the bulk liquid concentration), as shown in eq 9. The two film resistance model was used to calculate the overall gas mass transfer coefficient eq 10, where the phase equilibrium constant (m) and the local mass transfer coefficients in both phases (k_{G,CO_2}, and k^{rxn}_{L,CO_2}) are needed. Here, the local mass transfer coefficient in the liquid phase has the superscript rxn to differentiate the coefficient in the reactive liquid phase from that in the nonreactive liquid phase (without superscript).

$$\dot{N}_{CO_2} = K_{L,CO_2}(c^*_{CO_2} - c_{CO_2}) = K_{G,CO_2}(y_{CO_2} - y^*_{CO_2})\frac{P}{RT} \tag{9}$$

$$\frac{1}{K_{G,CO_2}} = \frac{1}{k_{G,CO_2}} + \frac{m}{k^{rxn}_{L,CO_2}} \tag{10}$$

The equilibrium concentration of CO_2 ($c^*_{CO_2}$) was calculated from the isofugacity equation by assuming an ideal gas phase (fugacity coefficient set to 1) and Henry's law, as shown in eq 11. The phase equilibrium constant is calculated using eq 12, which considers liquid and gas concentrations in $kmol/m^3$ and reformulates eq 11. For taking the presence of the ions in the liquid phase (nonideality of the liquid phase) into account, Henry's volatility constant ($H^m_{CO_2}$) was calculated from the ion concentrations (c_{Na}, c_{OH}, c_{CO_3}) and Henry's volatility constant

https://doi.org/10.1021/acs.iecr.3c00357
Ind. Eng. Chem. Res. 2023, 62, 7566−7579

of the infinite diluted system (solubility of CO_2 in pure water), as shown in eq 13. Henry's volatility constant of CO_2 in pure water ($H^{\infty}_{CO_2}$) was a function of the system temperature as reported in the literature,[22] and the parameters of eq 13 were taken from a study of gas solubility in salt solutions.[23]

$$c^{*}_{CO_2} H_{CO_2} = y_{CO_2} P \tag{11}$$

$$m = \frac{c_G}{c^{*}_{CO_2}} = \frac{y_{CO_2} P/RT}{c^{*}_{CO_2}} = \frac{H_{CO_2}}{RT} \tag{12}$$

$$H_{CO_2} = H^{\infty}_{CO_2} \times 10^{[(h_{Na}+h_g)c_{Na}+(h_{OH}+h_g)c_{OH}+(h_{CO_3}+h_g)c_{CO_3}]} \tag{13}$$

The local gas mass transfer coefficients for the both gas and liquid phases (non reactive) were calculated with correlations proposed in the literature,[24] which can be found in Section S.3, Supporting Information. The local gas mass transfer coefficient was a direct function of the inner circulating gas flow rate ($\dot{F}_{circ}$). The local mass transfer coefficient in the liquid reactive phase is calculated using the enhancement factor (E) (eq 14), which considers the improvement of mass transfer in the liquid phase caused by the chemical reaction (eq 2). The enhancement factor is usually a function of the Hatta number, which was calculated with eq 15. This equation was obtained from the two film theory, k' refers to the pseudo-first-order kinetic constant, D_{L,CO_2} is the diffusivity of CO_2 in the liquid mixture, and the k_{L,CO_2} is the mass transfer coefficient without the reaction.[25]

$$E = \frac{k^{rxn}_{L,CO_2}}{k_{L,CO_2}} \tag{14}$$

$$Ha = \frac{\sqrt{k' D_{L,CO_2}}}{k_{L,CO_2}} \tag{15}$$

Although the soda ash production is reported to be a two-step reaction (eqs 2 and 3), only the reaction rate of eq 2 was considered in the model because it can be assumed that the second step reaction (eq 3) is very fast and the overall reaction rate is only limited by the first step reaction.[26] The kinetics of the overall reaction can be described with a second-order reaction rate expression (eq 16) or a pseudo-first-order reaction rate expression with reference to the dissolved gas concentration (eq 17). Here, k' is the pseudo-first-order kinetic constant that is calculated as shown in eq 18. In addition, the reaction is considered irreversible because the hydroxide ion concentration in this work is much higher than the concentration of dissolved CO_2.[26] NaOH was above 0.5 M, which results in a molar ratio of more than 5000 OH^-/CO_2 in the liquid phase. Moreover, according to the model calculations, the CO_2 concentration in the liquid phase is practically zero since the reaction is very fast, and as soon as CO_2 is dissolved, it reacts with the hydroxide ions.

$$r = k c_{CO_2} c_{OH^-} \tag{16}$$

$$r = k' c_{CO_2} \tag{17}$$

$$k' = k c_{OH^-} \tag{18}$$

Different expressions for the calculation of the enhancement factor have been proposed depending on the Hatta number value (reaction regime).[27] For pseudo-first-order irreversible reactions that are very fast compared to the mass transfer phenomena, $Ha > 3$ and $E = Ha$. In our model, the Hatta number was evaluated and proven to be always over this limit. Therefore, eqs 14 and 15 can be equalized, and k^{rxn}_{L,CO_2} can be calculated from the pseudo-first-order kinetic constant and the diffusivity of CO_2 in the liquid mixture, as shown in eq 19.

$$k^{rxn}_{L,CO_2} = \sqrt{k' D^{L,m}_{CO_2}} \tag{19}$$

By replacing eqs 12 and 19 in eq 10, a general expression is obtained to calculate the liquid overall mass transfer coefficient shown in eq 20. For the calculation of k_{L,CO_2} and $D^{L,m}_{CO_2}$, the expressions used in the literature[28] were applied. According to them, the diffusivity of CO_2 ($D^{L,m}_{CO_2}$) in the mixture solution ($D^{L,m}_{CO_2}$) is a function of the viscosity of the mixture, the viscosity of pure water and the diffusivity of CO_2 in pure water (the diffusivity in pure water was calculated as a function of temperature[13]). From the model analysis, it was observed that $D^{L,m}_{CO_2}$ is a key parameter heavily affecting the results, and it should be determined with high precision. Therefore, viscosity measurements of solutions containing NaOH and Na_2CO_3 were performed using a falling-ball viscometer and compared with the predictions of a literature correlation.[29] After observing deviations around 27%, a specific empirical correlation was obtained for a proper description of this property with deviations around 3% (see Section S.3, Supporting Information).

$$\frac{1}{K_{G,CO_2}} = \frac{1}{k_{G,CO_2}} + \frac{H_{CO_2}}{RT\sqrt{k' D^{L,m}_{CO_2}}} \tag{20}$$

In a system where the mass transfer in the gas phase is not limiting, eq 20 can be transformed into eq 21. In such a case, the overall mass transfer coefficient does not depend on the calculation of the local mass transfer coefficients. In other words, the overall mass transfer coefficient is independent of the flow regime and is only dependent on chemical parameters (reaction kinetics and diffusivity).

$$K_{G,CO_2} = \frac{RT}{H_{CO_2}} \sqrt{k' D^{L,m}_{CO_2}} \tag{21}$$

The reaction rate was not calculated in activities since the nonidealities caused by the ions were considered in the calculation of the reaction rate constant (k), as shown in eq 22. In this expression, the infinite dilution reaction rate constant (k^{∞}) and the ionic strength of the solution are needed (I_{Na}, I_{OH}, I_{CO_3}). This function and its parameters were previously reported in the literature for the considered system.[18]

$$k = k^{\infty} \times 10^{[b_{Na} I_{Na} + b_{OH} I_{OH} + b_{CO_3} I_{CO_3}]} \tag{22}$$

The water flux ($\dot{N}_w$) was calculated from the local gas mass transfer coefficient of water ($k_{G,w}$) and the gas concentration gradient (assuming that the interphase is in equilibrium with the bulk concentration in the liquid phase), as shown in eq 23. Here, the main assumption is that the mass transfer resistance on the liquid phase is negligible. The equilibrium gas concentration of water (y^{*}_w) is calculated from eq 24, where the activity of water (a_w) is a function of the NaOH and Na_2CO_3 concentrations and temperature and p_s is the vapor pressure of pure water calculated with the function reported in

https://doi.org/10.1021/acs.iecr.3c00357
Ind. Eng. Chem. Res. 2023, 62, 7566−7579

Table 2. Overview of Experimental Parameters and Obtained Ranges of Steady-State CO_2 Concentration in the Gas Phase and Mass Transfer Coefficients

run no.	inlet flow CO_2, $\dot{F}_{in}$ (μL/min)	NaOH concentration, c_{NaOH} (wt %)	reactor volume (mL)[a]	temp., T (°C)	area, S (m^2)	circulating gas flow, $\dot{F}_{circ}$ (L/min)	steady-state CO_2 conc. y_{CO_2} (ppm)	experimental mass transfer coefficient, K_{G,CO_2} (mm/s)
1	312−1057	3.007	316	15	0.003144	0.7	689−2543	2.35−2.47
2	312−1057	5.28	316	15	0.003144	0.7	670.5−2491	2.40−2.57
3	312−1057	10.06	316	15	0.003144	0.7	715.9−2591	2.31−2.54
4	312−1057	15.10	316	15	0.003144	0.7	916.15−3238	1.83−1.98
5	312−1057	30.11	316	15	0.003144	0.7	3259−11 000	0.48−0.53
6	153−1057	6.09	143	15	0.001739	0.7	518.1−3817	2.85−3.07
7	153−1057	6.06	316	15	0.003144	0.7	304−2254	2.68−2.89
8	153−1057	6.09	628	15	0.004761	0.7	219−1539	2.59−2.80
9	153−1057	6.011	1187	15	0.006666	0.7	142−1237	2.42−2.90
10	312	6.28	1187	15	0.006666	0.4−1.6	310.2−377.57	2.11−2.74
11	312 and 738	5.99	143	5−20	0.001739	0.7	715.61−3438.4	2.03−4.5
12	312 and 738	4.68[b]	143	15	0.001739	0.7	2180−4306.6	1.71−3.47

[a]Used reactor volume, which changes the gas volume and the surface area. [b]Experiments with initial Na_2CO_3 in the liquid phase: 0−11.01 wt %.

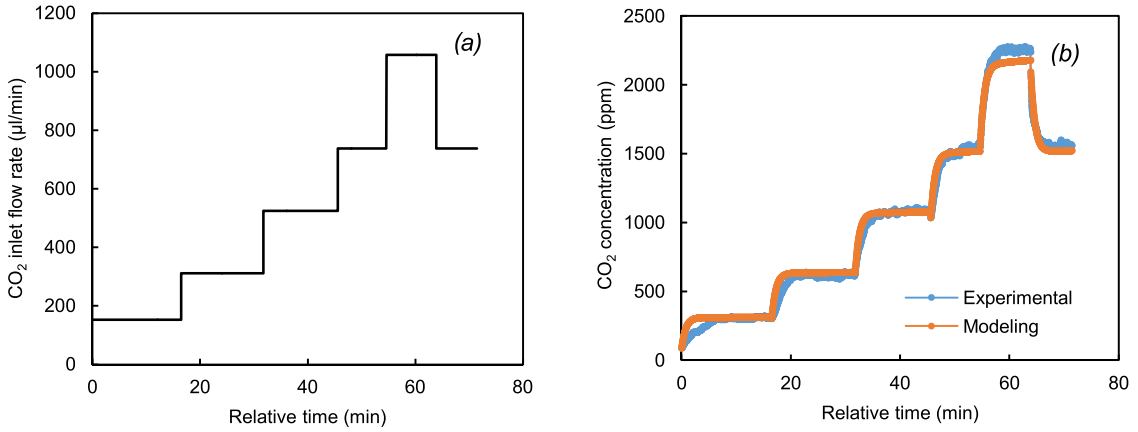

Figure 4. Results of exp. 7 (Table 2). (a) Step changes in the inlet flow rate of CO_2 to the system and (b) CO_2 concentration of the gas phase during the experiment with 6 wt % NaOH, a 0.003144 m^2 mass transfer area, and 0.7 L/min circulating flow rate.

the literature.[23] Here, the activity of water was calculated using a polynomic correlation obtained from Aspen Plus V12 simulations using the ELECT-NRTL model. The specific obtained correlation is provided in Section S.3, Supporting Information.

$$\dot{N}_w = \frac{P}{RT} k_{G,w}(y_w^* - y_w) \tag{23}$$

$$a_w p_{s,w} = y_w^* P \tag{24}$$

For the liquid phase, only component balances were done (see eqs 25 and 26), and the total concentration was calculated as the sum of all components' concentrations. The reaction term was taken out from the balances because the reaction rate was so high that the CO_2 concentration in the liquid bulk was practically zero all of the time (maximum 0.1% of the equilibrium concentration). The change in concentration of the reaction species is then driven mainly by the flux of CO_2 and water from and into the gas phase, respectively.

$$V_L \frac{dc_{CO_2}}{dt} = \dot{N}_{CO_2} S \tag{25}$$

$$V_L \frac{dc_w}{dt} = -\dot{N}_w S + V_L \frac{dc_{CO_2}}{dt} \tag{26}$$

$$\frac{dc_{NaOH}}{dt} = -2\frac{dc_{CO_2}}{dt} \tag{27}$$

$$\frac{dc_{Na_2CO_3}}{dt} = \frac{dc_{CO_2}}{dt} \tag{28}$$

The differential equations eqs 5−7 and 25−28 were solved simultaneously in Python, and the results were compared to the experimental data.

3. RESULTS AND DISCUSSION

A set of 12 experiments were performed in which either the NaOH concentration (c_{NaOH}), the mass transfer surface area (S), the inner circulating flow ($\dot{F}_{circ}$), the temperature (T), or the Na_2CO_3 concentration ($c_{Na_2CO_3}$) was changed, as shown in Table 2. For all experiments, except run number 10, the inlet flow of CO_2 was changed stepwise along the run within the ranges reported in Table 2. More detailed information on each experiment can be found in Sections S.2 and S.5, Supporting Information.

An example of a gas concentration profile along experiment 7 (exp. 7.1−7.6 in Section S.6) is shown in Figure 4, where the step changes on the inlet flow rate of CO_2 are also displayed. As seen, a few minutes after a step-change in the CO_2 feed rate, the absorption rate and the CO_2 feed rate were equal, and the

https://doi.org/10.1021/acs.iecr.3c00357
Ind. Eng. Chem. Res. 2023, 62, 7566−7579

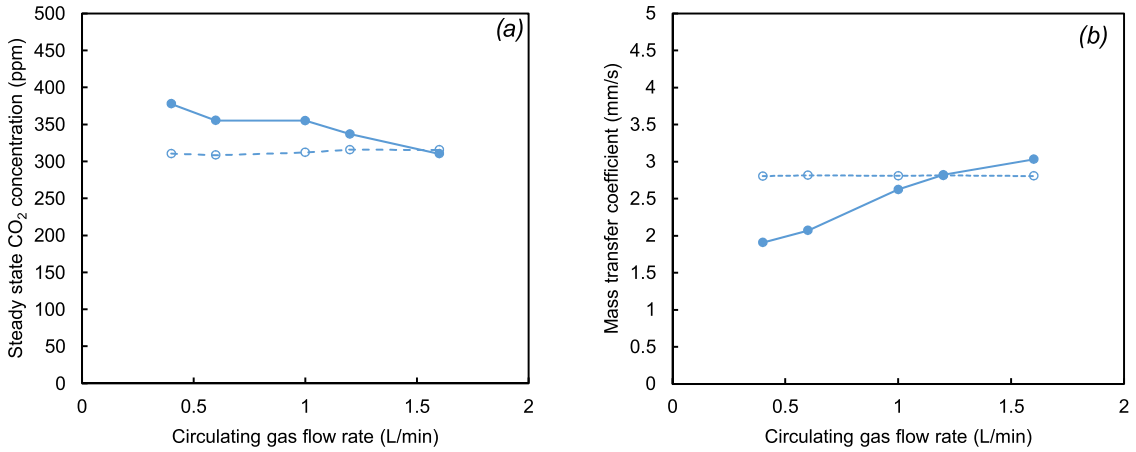

Figure 5. Effect of the circulating gas flow rate on the (a) steady-state CO_2 concentration and (b) mass transfer coefficient at 312 μL/min CO_2 entering the system. Experimental (solid line) and model (dashed line) values.

CO_2 concentration shown on the gas analyzer reached a steady state. It should be noted that the steady-state gas concentrations in Table 2 correspond to the average of recorded CO_2 concentration values for at least 5 min. The steady-state CO_2 concentration of two experiments having the same inlet flow rate of CO_2 can be compared.

Besides the steady-state CO_2 concentration, the mass transfer coefficient (K_{G,CO_2}) was used to evaluate the absorption process. In the model, the overall mass transfer coefficient was finally calculated using only the local mass transfer coefficient in the liquid phase using eq 21 (instead of considering the local mass transfer coefficients of both liquid and gas phases). By neglecting the resistance for mass transfer in the gas phase, the modeled data were closer to the experimental data (the average absolute error for all experiments changed from 303.6 ppm, considering k_{G,CO_2}, to 203.4 ppm, neglecting it). This might indicate that in the setup used, the CO_2 steady-state concentration was underdetermined, which is in agreement with the expected experimental errors described in Section 2.2. Thus, the mass transfer in the gas phase was neglected in the model because of the experimental uncertainties.

The experimental overall mass transfer coefficient was calculated with eq 29, which was deduced from the mass balance of CO_2 in the gas phase eq 6 and the flux equation eq 9. Here, the term $\Delta y_{CO_2}/\Delta t$ was calculated for each CO_2 feed rate step using the initial and steady-state CO_2 concentration; $y^{in}_{CO_2}$ was always 1 because the feed gas was pure carbon dioxide, and y_{CO_2} corresponded to the steady-state concentration of each CO_2 feed rate step. The gas mass transfer coefficient was used to obtain a performance indicator calculated only with measured values. This parameter was compared with the theoretical value obtained from eqs 20 and 21. The values generated in the present study are between 0.48 and 3.06 mm/s, which are of the same order of magnitude as those obtained in similar studies with 0.15−2.6 mm/s.[6]

$$K^{exp}_{G,CO_2} = \frac{\left(y^{in}_{CO_2}\dot{F}_{in} - \frac{PV_G}{RT}\frac{\Delta y_{CO_2}}{\Delta t}\right)}{Sy_{CO_2}\left(\frac{P}{RT}\right)} \quad (29)$$

For each CO_2 feed rate step in each experiment, the relative root-mean-square error (RRMSE) in the description of the gas phase CO_2 concentration and relative error (RE) of the steady-state CO_2 concentration were calculated according to eqs 30 and 31. Here, ND is the number of data points recorded at one CO_2 feed rate step (reported in Table S1 of the SI). While the RRMSE includes the dynamic information of each experiment, the RE only considers the steady-state condition. Both error values obtained for each feed rate step are reported in the Supporting Information (Table S2). The average RRMSE for all experiments was 19.61% (2.02−260%). The biggest deviation was probably caused by the inability of the model to describe the start-up of the setup (a more detailed model describing the filling of the whole volume space would be required). In contrast, a better description of the steady-state CO_2 concentration expressed by an RE between 0.44 and 48.5% was found. The average absolute relative deviation (AARD) of steady-state concentration was 9.49%. This error value is inside AARD reported for the thermodynamic and kinetic parameters used (7.1% for Henry's constant parameters[30] and 11.6% for kinetic parameters[18]).

$$\text{RRMSE}\ (\%) = \sqrt{\frac{\sum_i^{ND}\left(\frac{y^{exp}_{CO_2,i} - y^{mod}_{CO_2,i}}{y^{exp}_{CO_2,i}}\right)^2}{ND}} \times 100 \quad (30)$$

$$\text{RE}\ (\%) = \frac{y^{exp}_{CO_2} - y^{mod}_{CO_2}}{y^{exp}_{CO_2}} \times 100 \quad (31)$$

A qualitative comparison between the experimental and model CO_2 concentration profile can be obtained from Figure 4b. It can be observed that the model has a good prediction capability in terms of the steady-state CO_2 concentration, especially at low inlet flow rates of CO_2. Although at these conditions, there is a slight deviation in the dynamic characteristic of the system, the prediction of the steady-state values is considered at this point of the study more important. A comparison between the experimental and model profiles for each feed rate step in each experiment is presented in the Supporting Information (Figures in Section S.7).

In general, the model shows a good predictive capability, and some of the assumptions were numerically proven. For example, Hatta numbers were practically always above 3, and the mass transfer coefficients in the gas phase were bigger than in the liquid phase (at least 22 times bigger). From the model,

https://doi.org/10.1021/acs.iecr.3c00357
Ind. Eng. Chem. Res. 2023, 62, 7566−7579

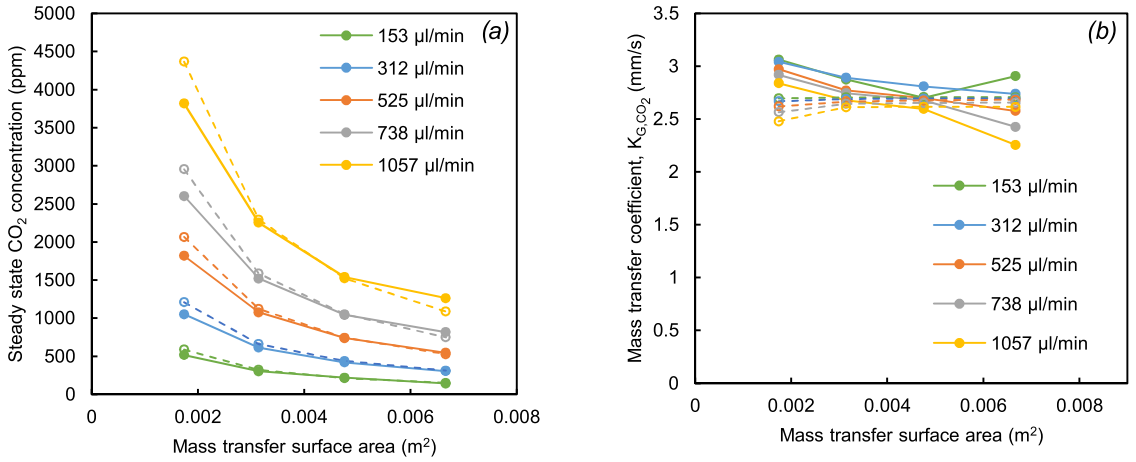

Figure 6. Effect of the mass transfer surface area on the (a) steady-state CO_2 concentration and (b) mass transfer coefficient with different feeding rates of CO_2. Experimental (solid line) and model (dashed line) values.

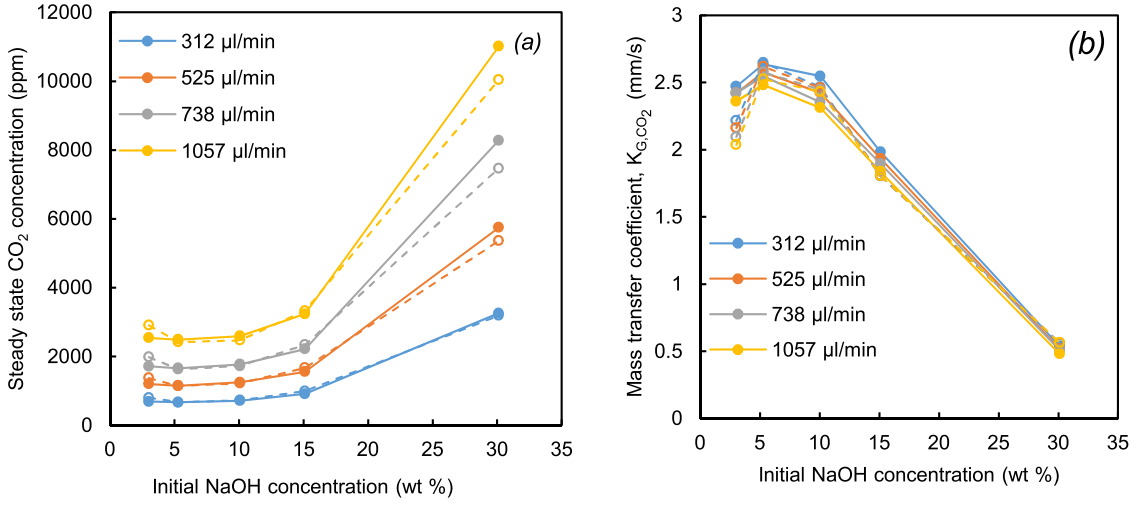

Figure 7. Effect of the NaOH concentration on the (a) steady-state CO_2 concentration and (b) mass transfer coefficient with different feeding rates of CO_2. Experimental (solid line) and model (dashed line) values.

it was observed that, due to the reaction, the concentration gradient for mass transfer is always the highest possible. Consequently, the flux of CO_2 (that is, the rate of absorption in kg $CO_2/(m^2 \cdot h)$) is mainly affected by the steady-state concentration (influenced by the pressure, the feeding rate, the temperature, and the ion concentrations) and the kinetic constant (influenced by the temperature and the ion concentrations). To identify the most important parameters on the performance of the absorption process, the effect of some operational and process design variables was analyzed and is discussed as follows.

3.1. Experimental Evaluation of Operating Conditions. Some experiments were done initially to study how the size of the reactor and the circulating gas flow rate inside the loop affects the steady-state CO_2 concentration and mass transfer coefficient. Using the second setup mentioned before in Section 2.2 and presented in Section S.1 (Supporting Information), different circulation flow rates, $\dot{F}_{circ}$, were tested in the absorption loop to study the changes in the gas steady-state concentration during run 10 (Table 2). As depicted in Figure 5, the steady-state CO_2 concentration and, consequently, the mass transfer coefficient are influenced by the circulating gas flow rate in the lower range. This indicates the absorption of CO_2 is controlled by the mass transfer in the gas phase at low circulating flow rates. The difference between the experimental and modeling results leads to the hypothesis about the imperfect mixing in the gas phase at low circulating gas flow rates. The observed overestimation of the modeled mass transfer coefficients (and the respective underestimation of the steady-state CO_2 concentrations) might be because of the assumption of the ideal mixing in the gas phase that was better obtained at high circulating gas flow rates. Nevertheless, for the rest of the experiments, the setup depicted in Figure 2 with a flow rate of 0.7 L/min was used.

To study the effect of the mass transfer surface area, S, on the absorption performance, four different reactors in runs 6, 7, 8, and 9 (Table 2) with different sizes and surface areas in the range of 0.0017−0.0066 m^2 were used. The NaOH concentrations were identical in these runs. The results are presented in Figure 6, where the lowest steady-state CO_2 concentration is obtained with the biggest surface area. This trend was expected since more CO_2 can be captured while the surface area is increased. On the other hand, as shown in Figure 6b, the modeled mass transfer coefficients show no significant dependence on the mass transfer area because they are, by definition, normalized to the surface area. Slight

https://doi.org/10.1021/acs.iecr.3c00357
Ind. Eng. Chem. Res. 2023, 62, 7566−7579

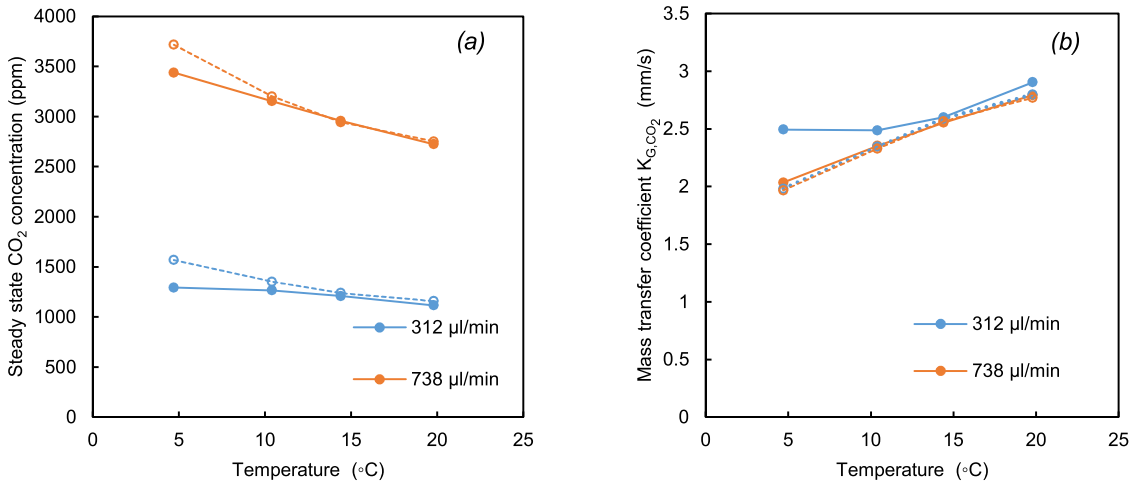

Figure 8. Effect of temperature (experiments 11.6−11.13) on the (a) steady-state CO_2 concentration and (b) mass transfer coefficient at 312 and 738 μL/min CO_2 entering the system. Experimental (solid line) and model (dashed line) values.

deviation of the model from the ideal behavior occurs from differences in the modeled solution compositions. However, also the obtained experimental mass transfer coefficients are slightly affected by the mass transfer surface area, which might be attributed to the experimental errors which were discussed before.

3.2. Effect of NaOH Concentration, c_{NaOH}. To study the effect of the reactant concentration in the solution, five different concentrations between 3 and 30 wt % of NaOH (0.7−10 M) have been used. The results of the experiments and the model on the steady-state CO_2 concentration and the mass transfer coefficient are presented in Figure 7. For all inlet flow rates, the smallest steady-state CO_2 concentration and the highest mass transfer coefficient are obtained with a NaOH concentration of around 6 wt % (1.6 M). This result shows that higher hydroxide ion concentrations do not necessarily result in better absorption performance. Similar behavior was theoretically calculated and reported in the literature before,[6] where it was discussed that the increase of OH^- ion concentration (ionic strength) results in the reduction of the diffusivity and solubility of CO_2 in the liquid phase. However, in the cited work, above 1.5 M NaOH concentration, the mass transfer coefficient was relatively insensitive to the NaOH concentration. This phenomenon had been only experimentally measured and analyzed in a system with high CO_2 concentration (pure CO_2 in the gas phase), where the optimal NaOH concentration was around 4 M (15 wt %) and the obtained optimal mass transfer coefficient was 0.5 mm/s.[20] Even though very small hydroxide ion concentrations cause a reduction of the pseudo-first-order kinetic constant in eq 18, at very high NaOH concentrations, the kinetic effect seems to be less important for absorption. The high ion concentration in the solution reduces the solubility of CO_2 in the liquid phase ("salting-out" effect) and reduces its diffusion rate due to the increase in the solution's viscosity.[29] The salting-out effect is also observed in eq 13, where Henry's volatility constant has a direct exponential dependence on the NaOH concentration. Consequently, the increment in the OH^- concentration does not represent any more an improvement of the absorption. The optimal NaOH concentration is then a condition in which the opposite influence of the hydroxide ions on the thermodynamic and physical properties and the kinetics is balanced. The quantified effect of diffusivity, Henry's constant, and the kinetic rate on the overall mass transfer coefficient is shown in Section S.8.

Deviations between the model and the experimental result in Figure 7 are related to the error of the parameters used (7% of error for Henry's constant and 12% for reaction kinetics). Figure 7b shows the effect of sodium hydroxide concentration on the mass transfer coefficient. The presence of the optimal concentration is more evident here because the mass transfer coefficient is not heavily affected by the inlet flow rate of CO_2 (which strongly affects the steady-state CO_2 concentrations).

3.3. Effect of Temperature. Studying the effect of temperature is crucial in DAC systems because they depend on weather conditions. It was investigated within run 11 (Table 2) at three different temperatures, in the range between 5 and 20 °C, which is outside the typical ranges studied in the literature. Higher temperatures have not been chosen because the average temperature during the year in Magdeburg (mid-Germany) is 10 °C, and the experimental setup was limited to room temperature in order to prevent water condensation in tubings outside the reactor. Figure 8a demonstrates that increasing the temperature improves the absorption performance. From the model point of view, temperature affects $H^{\infty}_{CO_2}$ (Henry's volatility constant of CO_2 in pure water), k^{∞} (the infinite dilution reaction rate constant), and D_{L,CO_2} (to the diffusivity of CO_2 in the liquid mixture) in eqs 13, 21, and 20, respectively. For calculating D_{L,CO_2}, the viscosity of mixture solutions was measured in the used temperature range. The absorption is improved at higher temperatures because the enhancement in the reaction rate and the liquid diffusivity is bigger than the decrease of the gas solubility (higher Henry's volatility constant). Consequently, as shown in Figure 8b, mass transfer coefficients are increased at higher temperatures when the solution is undersaturated and low in Na_2CO_3. Increasing the temperature from 5 to 20 °C improves K_{G,CO_2} by a factor of 1.5, which should be considered in the process design.

In Figure 8b, it can be observed that the modeled mass transfer coefficient is independent of the inlet CO_2 flow rate (also observed in Figure 7b). However, the deviation between the experimental and model K_{G,CO_2} is magnified at lower inlet flow rates. This is related to the numerical influence that both the steady-state CO_2 concentration and inlet flow rate have on

https://doi.org/10.1021/acs.iecr.3c00357
Ind. Eng. Chem. Res. 2023, 62, 7566−7579

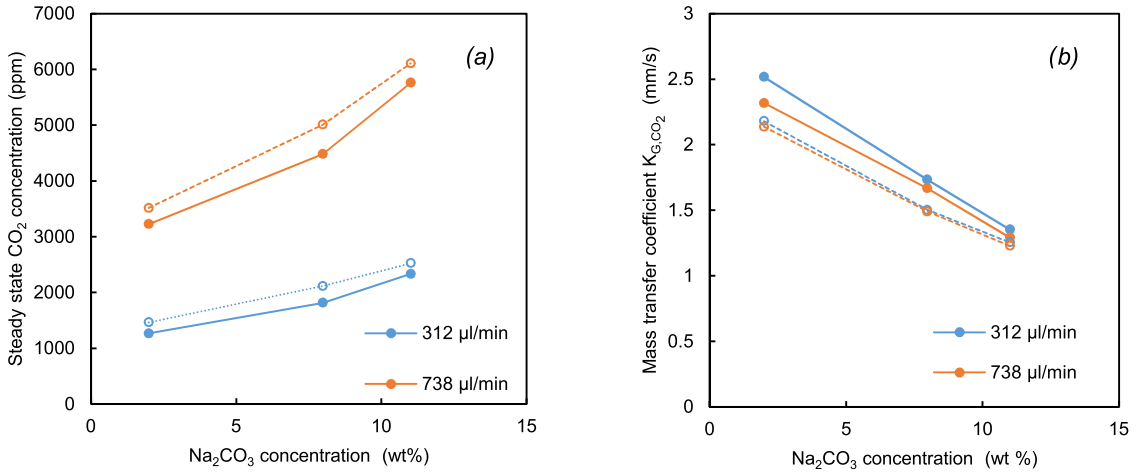

Figure 9. Effect of sodium carbonate concentration (experiments 12.4−12.9) on the (a) steady-state CO_2 concentration and (b) mass transfer coefficient in a solution containing 4.7 wt % NaOH. Experimental (solid line) and model (dashed line) values.

the mass transfer coefficient (eq 29). At lower flow rates, a big deviation of the steady-state CO_2 concentration results in a bigger deviation of the mass transfer coefficient (the error is not compensated by the flow rate).

3.4. Effect of Initial Sodium Carbonate Concentration. Although all industrial processes involving liquid DAC systems need to recycle liquid streams containing carbonate ions as feed to the absorber,[14,17] there are no studies evaluating the influence of this ion on the absorption performance. Since the future DAC system within this project is designed to also absorb up to saturation concentrations of sodium carbonate in sodium hydroxide solution, Na_2CO_3 concentration was changed in the range between 0 and 11 wt % in run 12. The upper range value was selected considering that the saturation concentration of sodium carbonate under the experimental conditions used (sodium hydroxide concentration is 4.8 wt % at 15 °C) is 10.1 wt %.[31] The results of the experiments, depicted in Figure 9a, reveals a decrease in absorption rate with increasing sodium carbonate concentration, which might be explained by the salting-out effect of ions. If the solution used for the absorption is saturated with Na_2CO_3, the mass transfer coefficient decreases by 50% (see Figure 9b). The obtained model data are in good fit with experimental ones; observed deviations might be related to both experimental and model errors.

3.5. Aspects of the Absorber Design. The modeled mass transfer coefficient K_{G,CO_2} reported in this work was independent of the geometry of the system and hydrodynamic conditions like liquid and gas velocities (see Section 3.1) and was only affected by the chemical interactions in the system (phase equilibria and kinetics). Thereby, it can be considered as the maximum mass transfer coefficient at applied conditions (temperature, NaOH, Na_2CO_3 concentrations, and CO_2 steady-state concentrations) independent of the type of absorber. The mass transfer coefficients obtained in this work are in the range of 0.5−3.1 mm/s, neglecting two experimental outliers. Changes in K_{G,CO_2} affect the height of the transfer unit $H_{OG} = w_G/(K_G a_e)$, (w_G is the gas velocity in the absorber, $K_G a_e$ is the volumetric mass transfer coefficient, and a_e is the specific surface area for mass transfer), which is directly related with the height of the absorber. For example, by changing NaOH from 15 wt % to the optimal amount obtained in this work, the absorber height would be reduced about 80%. Other conditions, like temperature and sodium carbonate concentration, which are more relevant to our work, also directly affect the height of the absorber. Moreover, the quantification of the effect of using saturated solutions of Na_2CO_3 on the mass transfer coefficient is important because it leads to a strong decrease in the absorption performance at elevated temperatures (>20 °C), as it is shown in Figure 10. At

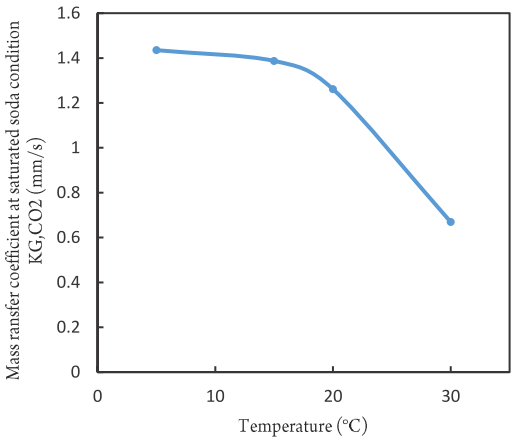

Figure 10. Modeled values of the mass transfer coefficient of CO_2 as a function of temperature at saturated Na_2CO_3 concentrations and 5 wt % NaOH.

temperatures below 30 °C, the solubility of sodium carbonate decreases significantly by decreasing the temperature. For example, changing the temperature from 5 to 20 °C at a constant NaOH concentration (e.g., 5 wt %) and saturated Na_2CO_3 concentration (possible operating CODA conditions) would increase the height of the absorber by 14%. The mass transfer coefficient decreases from 1.4 to 1.2, as shown in Figure 10, because the saturation concentration of sodium carbonate increases from 4.9 to 13.5 wt %. These are important findings for the CODA project, where temperature variations will happen at least on a daily basis, and saturated Na_2CO_3 solutions would be fed to the absorber.

Further, the high absorption potential of a pure sodium hydroxide solution, which will be the feed of a continuous DAC plant, should be employed by the smart staging of a number of single absorbers connected in series on the liquor

https://doi.org/10.1021/acs.iecr.3c00357
Ind. Eng. Chem. Res. 2023, 62, 7566−7579

side and in parallel on the air side. The effect of impurities in air should be considered within the DAC process design. Thereby, using a simple simulation of an absorber, it was observed that the CO_2 absorption is not affected by the presence of SO_2 and NO_x in air because of their low concentrations in air, around 0.001 and 0.01 ppm, respectively. Assuming all of the SO_2 and NO_x gases are absorbed by an absorber with a G/L volumetric ratio of 30 000 (using 33.3 mL of 1 M NaOH to absorb 400 ppm CO_2 from 1 m^3 air), the resulting mass fraction of $NaNO_3$, $NaNO_2$, and $NaSO_4$ in the liquid phase is roughly less than 10^{-7}. On the other hand, the presence of produced ions in the liquid phase, like SO_3^{2-}, NO_2^-, and NO_3^-, should be considered in the crystallization process. These ions should be removed from the system either by purging or by crystallizing the corresponding sodium salts. However, given the small concentration of these ions (in comparison to the CO_3^{2-} concentration), the most probable treatment would be purging.

3.6. Model Improvements. Parameters used to calculate Henry's volatility constant and the reaction rate in the literature were obtained by fitting experimental information also containing K^+ and Li^+ ions.[18,23] With the aim of obtaining a better description of the experimental results, model parameters were refitted to the presented data (system with only Na^+ and CO_3^{2-}). For this, first, a sensitivity analysis was done to identify which parameters affect the deviations significantly. The AARD was reduced from 9.49 to 7.8% by changing the parameter values as reported in Section S.8, Supporting information. These parameters can be used for the process design in the range between 3−30 wt % NaOH, 5−20 °C, 0.0153−1.2 vol % CO_2, and 0−11 wt % Na_2CO_3, as used in this work. It should be noted that modeling results presented in this work are obtained with the literature parameter and not with the refitted parameters.

4. CONCLUSIONS

The absorption of CO_2 in NaOH−Na_2CO_3−H_2O solutions was experimentally studied and complementary modeled at the relevant DAC conditions for soda ash production. Thereby, diluted concentrations of CO_2 (0.0153−1.2 vol %), concentrations of the NaOH solution between 3 and 30 wt %, concentrations of Na_2CO_3 between 0 and 11 wt %, and temperatures between 5 and 20 °C were chosen. The obtained results were evaluated by the mass transfer coefficient, K_{G,CO_2}, which was governed by the resistance of mass transfer in the liquid phase, and the most important variables affecting it were the concentration of NaOH and Na_2CO_3 and temperature. The obtained mass transfer coefficients in this work were in the range of 0.5−3 mm/s, and it has the highest value when the optimal concentration of NaOH of about 6 wt % was used. Moreover, it was observed that the increase of NaOH concentration does not necessarily have a positive effect on the mass transfer coefficient, probably due to competition in the solubility between NaOH and CO_2. A dynamic process model was formulated based on published submodels and parameters that were derived from non-DAC process conditions for soda ash production. The literature-based model was evaluated for the DAC-relevant process conditions by assessing its ability to predict the obtained experimental data. It was found that the non-DAC literature-based model was able to predict the DAC-relevant experimental data with an average error of 9.49%. Fitting of some relevant model parameters could decrease the average error of prediction to 7.8%. Additionally, it was concluded that even at optimum NaOH concentration, changes in the Na_2CO_3 concentration up to saturation concentration and temperature can affect the theoretical height of an absorber by up to 80%. These effects have to be considered in the future absorber design as a prerequisite for the subsequent crystallization of soda ash as the target compound of the CODA project. While this study focused on understanding and quantifying the effect of operational parameters on the mass transfer coefficient, future work will focus on the enhancement of absorption through equipment design.

■ ASSOCIATED CONTENT

Supporting Information

The Supporting Information is available free of charge at https://pubs.acs.org/doi/10.1021/acs.iecr.3c00357.

More details on the obtained experimental and modeled results including steady-state CO_2 concentration, RRSME, relative error, absorption rate, mass transfer coefficient for each of experiments, correlations used in the model, the sensitivity analysis of the studied parameters, more information regarding model improvments, and a photograph of the used set-up (PDF)

■ AUTHOR INFORMATION

Corresponding Author

Somayyeh Ghaffari − *Max Planck Institute for Dynamics of Complex Technical Systems, Magdeburg 39106, Germany;* orcid.org/0009-0004-0516-9902; Phone: +49 391 6110 324; Email: ghaffari@mpi-magdeburg.mpg.de

Authors

Maria F. Gutierrez − *Max Planck Institute for Dynamics of Complex Technical Systems, Magdeburg 39106, Germany*

Andreas Seidel-Morgenstern − *Max Planck Institute for Dynamics of Complex Technical Systems, Magdeburg 39106, Germany;* orcid.org/0000-0001-7658-7643

Heike Lorenz − *Max Planck Institute for Dynamics of Complex Technical Systems, Magdeburg 39106, Germany;* orcid.org/0000-0001-7608-0092

Peter Schulze − *Max Planck Institute for Dynamics of Complex Technical Systems, Magdeburg 39106, Germany;* orcid.org/0000-0002-1089-746X

Complete contact information is available at: https://pubs.acs.org/10.1021/acs.iecr.3c00357

Funding

This publication was mainly funded by the BMBF (the German Federal Ministry of Education and Research) within KlimPro and FONA HYPERLINK "https://www.fona.de" (research for sustainability), with a grant number of 01LJ2003B. Open access funded by Max Planck Society.

Notes

The authors declare no competing financial interest.

■ ACKNOWLEDGMENTS

The authors acknowledge the financial support by the BMBF (No. 01LJ2003B). Further, we thank our industrial partner, the CIECH group, for their cooperation and the company SChPrEngCo for initiating the CODA project.

LIST OF SYMBOLS

a_w activity of water
b_{Na^+} ion specific parameter for the calculation of the second-order reaction rate constant in an electrolyte system (m^3/kmol)
b_{OH^-} ion specific parameter for the calculation of the second-order reaction rate constant in an electrolyte system (m^3/kmol)
$b_{CO_3^{2-}}$ ion specific parameter for the calculation of the second-order reaction rate constant in an electrolyte system (m^3/kmol)
$c^*_{CO_2}$ concentration of CO_2 in the liquid phase in equilibrium with the bulk gas phase concentration of CO_2 (kmol/m^3)
c_{CO_2} liquid mole concentration of CO_2 (kmol/m^3)
c_w liquid mole concentration of water (kmol/m^3)
c_{NaOH} liquid mole concentration of NaOH (kmol/m^3)
$c_{Na_2CO_3}$ liquid mole concentration of Na_2CO_3 (kmol/m^3)
D_{L,CO_2} diffusivity coefficient of CO_2 in the liquid phase mixture (m^2/s)
E enhancement factor
$\dot{F}_{in}$ inlet flow rate of gas (kmol/s)
$\dot{F}_{circ}$ circulating gas flow rate (L/min)
Ha Hatta number
H_{CO_2} Henry's constant to describe the solubility of CO_2 in the liquid phase mixture $\left(\text{kPa}\frac{\text{m}^3}{\text{kmol}}\right)$
h_g gas specific parameter for the Henry's constant in an electrolyte system (m^3/kmol)
$H^\infty_{CO_2}$ Henry's constant to describe the solubility of CO_2 in pure water $\left(\text{kPa}\frac{\text{m}^3}{\text{kmol}}\right)$
h_{Na^+} ion specific parameter for Henry's constant in an electrolyte system (m^3/kmol)
h_{OH^-} ion specific parameter for Henry's constant in an electrolyte system (m^3/kmol)
$h_{CO_3^{2-}}$ ion specific parameter for Henry's constant in an electrolyte system (m^3/kmol)
I_{Na^+} ionic strength of Na^+ (kmol/m^3)
I_{OH^-} ionic strength of OH^- (kmol/m^3)
$I_{CO_3^{2-}}$ ionic strength of CO_3^{2-} (kmol/m^3)
I_{NaOH} ionic strength of NaOH (kmol/m^3)
$I_{Na_2CO_3}$ ionic strength of Na_2CO_3 (kmol/m^3)
k second-order reaction rate constant in the electrolyte mixture (m^3/(kmol·s))
k' pseudo-first-order reaction rate constant in the electrolyte mixture (s^{-1})
k^{rxn}_{L,CO_2} local mass transfer coefficient of CO_2 in the reacting liquid phase (m/s)
k^∞ second-order infinite dilution reaction rate constant (m^3/(kmol·s))
k_{L,CO_2} local liquid mass transfer coefficient of CO_2 in a solution without the reaction (m/s)
$k_{G,w}$ mass gas transfer coefficient of water (m/s)
k_{G,CO_2} mass gas transfer coefficient of CO_2 (m/s)
K_{G,CO_2} overall gas mass transfer coefficient of CO_2 (m/s)
K^{exp}_{G,CO_2} experimental absorption gas mass transfer coefficient (mm/s)
m gas liquid equilibrium constant
n_G number of moles in the gas phase (kmol)
$\dot{N}_{CO_2}$ flux of CO_2 from the gas phase to the liquid phase (kmol/(s·m^2))
$\dot{N}_w$ flux of water from the liquid phase to the gas phase (kmol/(s·m^2))
P pressure in the gas phase (kPa)
$p_{s,w}$ saturation pressure of water (kPa)
RRMSE relative root-mean-square error (%)
R universal gas constant (kPa·m^3/(kmol·K))
S mass transfer surface area (cross-section surface area of bottles calculated from the internal diameter of the reactor) (m^2)
V_L volume of the liquid phase (m^3)
V_G volume of the gas phase (m^3)
$y^{in}_{CO_2}$ concentration of CO_2 in the inlet gas flow (mole fraction)
y^{in}_w concentration of water in the inlet gas flow (mole fraction)
y_{CO_2} bulk concentration of CO_2 in the gas phase (called steady-state CO_2 concentration in this work) (mole fraction)
y_w bulk concentration of water in the gas phase (mole fraction)
y^*_w equilibrium concentration of water in the gas phase (mole fraction)
$\Delta y_{CO_2}/\Delta t$ total change in the CO_2 concentration in the respective experiment time (s^{-1})

REFERENCES

(1) Climate NASA Overview: Weather, Global Warming and Climate Change, 04 April 04, 2023. https://climate.nasa.gov/resources/global-warming-vs-climate-change/#:~:text=Global%20warming%20is%20the%20long,gas%20levels%20in%20Earth's%20atmosphere.

(2) Kharecha, P. A.; Hansen, J. E. Implications of "peak oil" for atmospheric CO_2 and climate. *Global Biogeochem. Cycles* **2008**, *22*, No. GB3012.

(3) Lackner, K. S.; Brennan, S.; Matter, J. M.; Park, A.-H. A.; Wright, A.; Van Der Zwaan, B. The urgency of the development of CO_2 capture from ambient air. *Proc. Natl. Acad. Sci. U.S.A.* **2012**, *109*, 13156−13162.

(4) Czaplicka, N.; Konopacka-Łyskawa, D. Studies on the utilization of post-distillation liquid from Solvay process to carbon dioxide capture and storage. *SN Appl. Sci.* **2019**, *1*, No. 431.

(5) Wisniak, J. Sodium carbonate—From Natural Resources to Leblanc and Back. *Indian J. Chem. Technol.* **2003**, *10*, 99−112.

(6) Stolaroff, J. K.; Keith, D. W.; Lowry, G. V. Carbon dioxide capture from atmospheric air using sodium hydroxide spray. *Environ. Sci. Technol.* **2008**, *42*, 2728−2735.

(7) Gaur, A.; Park, J.-W.; Jang, J.-H.; Maken, S.; Lee, J.; Song, H.-J. Characteristics of alkaline wastewater neutralization for CO_2 capture from landfill gas (LFG). *Energy Fuels* **2009**, *23*, 5467−5473.

(8) Yoo, M.; Han, S.-J.; Wee, J.-H. Carbon dioxide capture capacity of sodium hydroxide aqueous solution. *J. Environ. Manage.* **2013**, *114*, 512−519.

(9) Mahmoudkhani, M.; Heidel, K.; Ferreira, J.; Keith, D.; Cherry, R. S. Low energy packed tower and caustic recovery for direct capture of CO_2 from air. *Energy Procedia* **2009**, *1*, 1535−1542.

(10) Salmón, I.; Cambier, N.; Luis, P. CO_2 Capture by Alkaline Solution for Carbonate Production: A Comparison between a Packed Column and a Membrane Contactor. *Appl. Sci.* **2018**, *8*, No. 996.

(11) Shim, J.-G.; Lee, D. W.; Lee, J. H.; Kwak, N.-S. Experimental study on capture of carbon dioxide and production of sodium bicarbonate from sodium hydroxide. *Environ. Eng. Res.* **2016**, *21*, 297−303.

(12) Tavan, Y.; Hosseini, S. H. A novel rate of the reaction between NaOH with CO_2 at low temperature in spray dryer. *Petroleum* **2017**, *3*, 51−55.

https://doi.org/10.1021/acs.iecr.3c00357
Ind. Eng. Chem. Res. 2023, 62, 7566−7579

(13) Pichler, T.; Stoppacher, B.; Kaufmann, A.; Siebenhofer, M.; Kienberger, M. Continuous Neutralization of NaOH Solution with CO_2 in an Internal-Loop Airlift Reactor. *Chem. Eng. Technol.* **2021**, *44*, 38−47.
(14) Keith, D. W.; Holmes, G.; Angelo, D. S.; Heidel, K. A process for capturing CO_2 from the atmosphere. *Joule* **2018**, *2*, 1573−1594.
(15) Mazzotti, M.; Abanades, J. C.; Allam, R.; Lackner, K. S.; Meunier, F.; Rubin, E.; Sanchez, J. C.; Yogo, K.; Zevenhoven, R.*Mineral Carbonation and Industrial Uses of Carbon Dioxide*, IPCC Special Report on Carbon Dioxide Capture and Storage; IPCC, 2005, pp 319−338.
(16) Holmes, G.; Keith, D. W. An air−liquid contactor for large-scale capture of CO_2 from air. *Philos. Trans. R. Soc., A* **2012**, *370*, 4380−4403.
(17) Baciocchi, R.; Storti, G.; Mazzotti, M. Process design and energy requirements for the capture of carbon dioxide from air. *Chem. Eng. Process.* **2006**, *45*, 1047−1058.
(18) Gondal, S.; Asif, N.; Svendsen, H. F.; Knuutila, H. Kinetics of the absorption of carbon dioxide into aqueous hydroxides of lithium, sodium and potassium and blends of hydroxides and carbonates. *Chem. Eng. Sci.* **2015**, *123*, 487−499.
(19) Azizi, F.; Kaady, L.; Al-Hindi, M. Chemical absorption of CO_2 in alkaline solutions using an intensified reactor. *Can. J. Chem. Eng.* **2022**, *100*, 2172−2190.
(20) Hitchcock, L. B. Rate of Absorption of Carbon Dioxide Effect of Concentration and Viscosity of Caustic Solutions. *Ind. Eng. Chem.* **1934**, *26*, 1158−1167.
(21) Tamhankar, Y.; King, B.; Whiteley, J.; McCarley, K.; Cai, T.; Resetarits, M.; Aichele, C. Interfacial area measurements and surface area quantification for spray absorption. *Sep. Purif. Technol.* **2015**, *156*, 311−320.
(22) Rumpf, B.; Xia, J.; Maurer, G. Solubility of Carbon Dioxide in Aqueous Solutions Containing Acetic Acid or Sodium Hydroxide in the Temperature Range from 313 to 433 K and at Total Pressures up to 10 MPa. *Ind. Eng. Chem. Res.* **1998**, *37*, 2012−2019.
(23) Weisenberger, S.; Schumpe, D. A. Estimation of gas solubilities in salt solutions at temperatures from 273 K to 363 K. *AIChE J.* **1996**, *42*, 298−300.
(24) Treybal, R. E. *Mass-Transfer Operations*; McGraw-Hill, 1981.
(25) Bird, R. B.; Stewart, W. E.; Lightfoot, E. N. *Transport Phenomena*, 2nd ed.; Wiley International, 2001.
(26) Danckwerts, P. V. *Gas−Liquid Reactions*; McGraw-Hill: New-York, 1970.
(27) van Swaaij, W.; Versteeg, G. Mass transfer accompained with complex reversible chemical reactions in gas-liquid systems. *Chem. Eng. Sci.* **1992**, *47*, 3181−3195.
(28) Kucka, L.; Kenig, E. Y.; Gorak, A. Kinetics of the gas-liquid reaction between carbon dioxide and hydroxide ions. *Ind. Eng. Chem. Res.* **2002**, *41*, 5952−5957.
(29) Laliberté, M. Model for calculating the viscosity of aqueous solutions. *J. Chem. Eng. Data* **2007**, *52*, 321−335.
(30) Gondal, S.; Asif, N.; Svendsen, H. F.; Knuutila, H. Density and N_2O solubility of aqueous Hydroxide and Carbonate Solutions in the temperature range from 25 to 80 C. *Chem. Eng. Sci.* **2015**, *122*, 307−320.
(31) Stephen, H.; Stephen, T. *Ternary Systems: Solubilities of Inorganic and Organic Compounds*; Elsevier, 2013.

https://doi.org/10.1021/acs.iecr.3c00357
Ind. Eng. Chem. Res. 2023, 62, 7566−7579